PHYSICAL REVIEW B **94**, 121202(R) (2016)

NV centers in 3*C*, 4*H*, and 6*H* silicon carbide: A variable platform for solid-state qubits and nanosensors

H. J. von Bardeleben,[1,*] J. L. Cantin,[1] A. Csóré,[2] A. Gali,[2,3] E. Rauls,[4] and U. Gerstmann[4]

[1]*INSP, Université Pierre et Marie Curie, UMR 7588 au CNRS 4 place Jussieu, 75005 Paris, France*

[2]*Department of Atomic Physics, Budapest University of Technology and Economics, Budafoki út 8, H-1111, Budapest, Hungary*

[3]*Wigner Research Centre for Physics, Hungarian Academy of Science, P. O. Box 49, Budapest H-1525, Hungary*

[4]*Department Physik, Universität Paderborn, Warburger Strasse 100, 33098 Paderborn, Germany*

(Received 31 March 2016; revised manuscript received 7 July 2016; published 26 September 2016)

The outstanding magneto-optical properties of the nitrogen-vacancy (NV) center in diamond have stimulated the search for similar systems. We show here that NV triplet centers can also be generated in all the main SiC polytypes. We have identified by electron paramagnetic resonance spectroscopy and first-principles calculations the axial NV^- pairs in 3*C*, 4*H*, and 6*H* SiC, showing polytype and lattice site-specific magnetic and optical properties. We demonstrate very efficient room-temperature spin polarization of the ground state upon near infrared optical excitation for the NV center in 3*C* SiC and axial NV centers in the hexagonal (4*H*, 6*H*) polytypes; the signals of basal pairs are much lower in intensity. Axial NV centers in hexagonal SiC polytypes and thus constitute unidirectional ensembles which may be useful in nanosensing applications.

DOI: 10.1103/PhysRevB.94.121202

Defects in solids carrying spins have recently become attractive systems for their application as qubits [1,2]. Particularly, the negatively charged nitrogen-vacancy defect in diamond [3], or briefly NV center, is a leading contender in quantum information processing applications [4]. This is related to the facts that its $S = 1$ ground state can be optically spin polarized and the intensity of its fluorescence depends on the initial spin state, i.e., its spin state can be optically initialized and read out [5,6]. The spin-polarization and readout processes are strongly interconnected via singlet states lying between the triplet states that are responsible for the spin-selective nonradiative transition from the triplet excited state to the ground state where the selection rules associated with its C_{3v} symmetry play a crucial role [7]. The optical spin polarization and readout are robust processes in NV centers of diamond; as they operate even at room temperature and above, they are suitable for application as qubits in quantum computing and can be employed as nanoscale sensors [6]. Despite the great success of NV centers in diamond, there is quest to find alternative qubit systems in technologically mature materials with magneto-optical properties optimal for the targeted application. It has been proposed [8–20] that silicon carbide (SiC) may host defects akin to the NV center in diamond. And very recently, a spin triplet in N-doped and electron-irradiated 4*H* SiC has been attributed to the direct NV equivalent, a ($V_{Si}N_C$) nearest-neighbor pair [21].

In this Rapid Communication, we report the assessment of (axial symmetric) NV centers in the three polytypes 4*H*, 6*H*, and 3*C* SiC, and determine their basic magnetic and optical properties. The total number of configurations in each polytype and their very similar spin-Hamiltonian parameters strongly support an assignment to ($V_{Si}N_C$) nearest-neigbor centers. In the 3*C* polytype, the direct equivalent of diamond, all nearest-neighbor defect pairs have C_{3v} symmetry and four equivalent [111]-oriented NV centers are expected and observed. In the hexagonal 4*H* and 6*H* crystals, *c*-axis-oriented (axial) NV centers coexist with basal, lower symmetry NV centers (cf. Fig. 1). Here, we show experimentally that the $^3A_2$ ground state of the axial configurations exclusively can be efficiently spin polarized by the near infrared (around 980 nm), giving rise to much higher electron paramagnetic resonance (EPR)-signal intensities. Hence, we focus in this study on the axial configurations which all have C_{3v} symmetry identical with that of the NV center in diamond. The attribution to specific lattice sites is thereby established by comparative DFT calculations of the triplet ground states and their characteristic spin-Hamiltonian parameters. As the spin polarization can even be obtained at room temperature this makes the axial symmetric NV centers in SiC very promising qubit candidates operating at the telecom-compatible near-infrared region, which would be also advantageous for *in vivo* biological nanosensor applications [22,23].

All of our first principles calculations were performed in the framework of density functional theory (DFT) using the semilocal Perdew-Burke-Ernzerhof (PBE) functional [24], projector augmented wave (PAW) potentials [25], periodic boundary conditions, and supercells containing up to 576 atoms. Based on fully relaxed ground-state geometries (forces below 0.01 eV/Å), we calculated the magnetic signature of the spin-triplet states of axial, negatively charged ($V_{Si}N_C$) pairs in 4*H*, 6*H*, and 3*C* SiC (cf. Table I). For the *g* tensors and hyperfine (HF) splittings we used the QUANTUM ESPRESSO package [26] and gauge-including (GI)PAW pseudopotentials [27] (see Ref. [21] for further details). Based on standard PAW potentials, the zero-field splitting (ZFS) parameters *D* associated with the electron spin dipole-dipole interaction are calculated with our house-built code [28,29], whereby the electron wave functions are taken from VASP code [30]. We employed 512-atom 3*C*, 576-atom 4*H*, and 432-atom 6*H* supercells within Γ-point sampling of the Brillouin zone. A plane-wave expansion of the wave functions with a cutoff of 420 eV provided nicely convergent ZFS tensors.

NV centers have not been observed in any as grown SiC materials. To generate them, we have irradiated 4*H*, 6*H*, and 3*C* nitrogen-doped *n*-type bulk monocrystals with high-energy

*vonbarde@insp.jussieu.fr

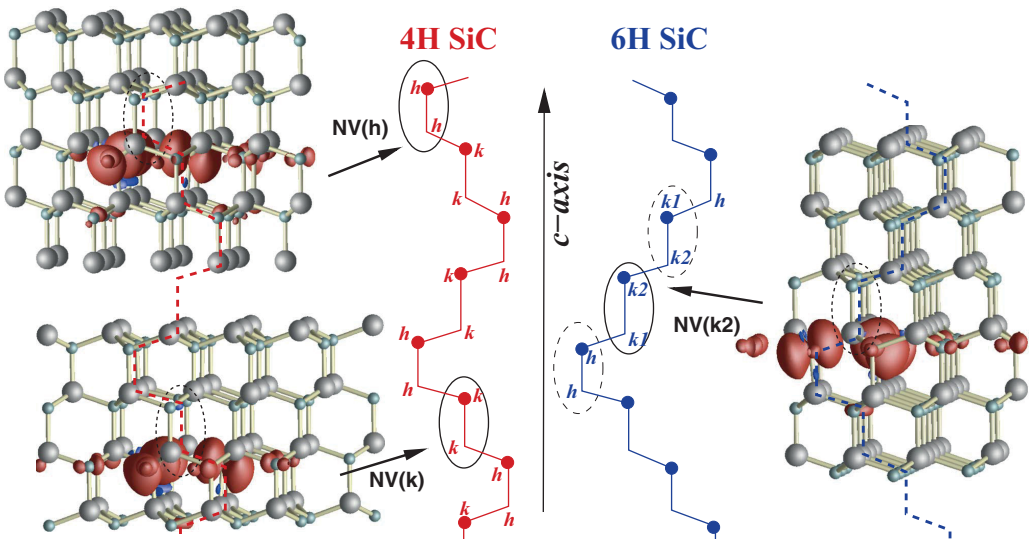

FIG. 1. Sketch of the axial $N_C V_{Si}$ (NV) pairs in $4H$ and $6H$ SiC. The spatial distributions of the spins are also given: They are dominated by the carbon dangling bonds of V_{Si}, with small negative component on the N atom giving rise to indirect hyperfine interaction observed in the EPR spectra.

(MeV) protons or electrons. In this first step, Si monovacancies are created. In a second step, the irradiated crystals have been thermally annealed in the 850 °C temperature range to allow the diffusion of Si vacancies and the formation of $(V_{Si}N_C)$ close pair centers [8,31]. The samples have been studied by EPR spectroscopy at X band and Q band in the 4 to 300 K temperature range. The spin Hamiltonian parameters were deduced from the angular variation of the EPR spectra for a rotation of the magnetic field in the (110) and (1100) planes for $3C$ and $4H$, $6H$ material, respectively.

In Fig. 2 we show the EPR spectrum observed in a proton irradiated and thermally annealed $3C$ SiC sample. In addition to $S = 1/2$ centers with g values close to 2.000, which will not be discussed here, we observe two dominant $S = 1$ spectra with C_{3v} symmetry. One of them is the known spectrum of the neutral divacancy, which has been published previously [32]; the second one is characterized by a resolved triplet structure indicative of HF interaction with a 100% abundant nucleus with a nuclear spin $I = 1$ (^{14}N). In most samples, this spectrum can be weakly observed already under thermal equilibrium conditions but its intensity is increased by a factor of 10 to 100 under IR photoexcitation (with up to 1305 nm), indicating an efficient ground-state spin polarization [21]. Notably, optically induced spin initialization is a characteristic property of NV centers in diamond, too. The spin Hamiltonian parameters of this defect ground state are determined from a conventional spin-triplet ($S = 1$) Hamiltonian:

$$H = \mu_B\, SgB + SDS + \sum_k (SA_kI_k + g_{N_k}\mu_N BI_k),$$

where all terms have their usual meanings [21]. From the angular variation of the EPR spectrum, we deduce the following main parameters: $D = 1303$ MHz, $g_\parallel = 2.004$, $g_\perp = 2.003$, $A_\parallel(^{14}\mathrm{N}) = \pm 1.26$ MHz ($T = 4$ K). Based on the excellent agreement of these values and the DFT-calculated spin Hamiltonian parameters (cf. Table I), we assign the $S = 1$ spectrum to the NV center in $3C$ SiC. In particular, the small but resolved HF interaction with one ^{14}N nearest neighbor nucleus discriminates these centers from electrically similar defects like the neutral divacancies $(V_{Si}V_C)^0$ [21,32].

The optically induced ground-state spin polarization is directly visible in the EPR spectrum shown in Fig. 2: The phases of the low-field and high-field EPR spectra are inverted, the low-field lines being in absorption and the high-field line

TABLE I. Experimental and calculated (DFT) spin Hamiltonian parameters for the axially symmetric NV^- pairs in various SiC polytypes; (g values, zero-field splitting D [MHz], isotropic nitrogen HF interaction A [MHz], and ^{29}Si SHF splittings $A_\parallel$ [MHz] for B ∥ c) if the ^{14}N nucleus occupies a cubic ($3C$-SiC), quasicubic ($k1$, $k2$; k) or hexagonal (h) lattice sites. D^{DFT} is calculated from the appropriate component of the electron spin dipole-dipole tensor [28,29]. Besides the given large ^{13}C SHF of the *three* carbon dangling bonds, further *six* ^{13}C SHF with smaller splittings (≈1 MHz below the 6 × Si value) are predicted.

$(N_CV_{Si})^-$	$g_\perp^{exp}$	$g_\parallel^{exp}$	$g_\perp^{DFT}$	$g_\parallel^{DFT}$	D^{exp}	D^{DFT}	A^{exp}(1 × N)	A^{DFT}(1 × N)	$A_\parallel^{DFT}$(6 × Si)	$A_\parallel^{DFT}$(3 × Si)	$A_\parallel^{DFT}$(3 × C)
$3C$ SiC	2.003	2.004	2.0029	2.0034	+1303	+1409	1.26	−1.08	8.00	10.30	70.28
$6H$ SiC, h	2.003	2.004	2.0029	2.0036	+1328	+1404	1.32	−1.08	8.41	10.32	68.52
$6H$ SiC, $k1$	2.003	2.004	2.0029	2.0035	+1278	+1348	1.21	−1.20	8.26	10.42	70.44
$6H$ SiC, $k2$	2.003	2.004	2.0029	2.0036	+1355	+1431	1.26	−1.06	9.01	11.11	62.18
$4H$ SiC, h	2.003	2.004	2.0029	2.0036	+1313	+1428	1.23	−1.09	8.14	10.36	68.97
$4H$ SiC, k	2.003	2.004	2.0029	2.0036	+1270	+1377	1.12	−1.15	9.05	11.05	62.70

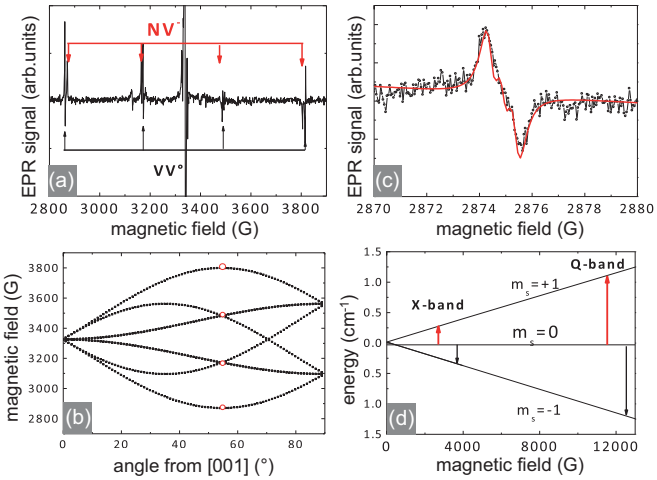

FIG. 2. 3C SiC: (a) EPR spectrum for B//[111] at $T = 4$ K under 980-nm photoexcitation displaying the NV and divacancy centers; (b) angular variation of the NV spectrum for a rotation of B in the (110) plane; red circles correspond to the spectrum shown in panel (a); (c) high-resolution spectrum of NV^- for B//[111] and its simulation (red) with three Lorentzian lines; and (d) energy level scheme for B//[111]; red (black) arrows indicate emission (absorption).

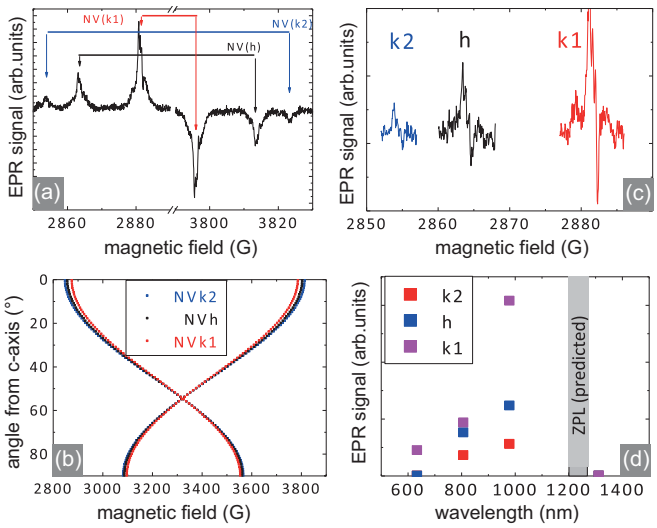

FIG. 3. 6H SiC: (a) NV EPR spectrum for B//c at $T = 4$ K (excitation with 980 nm); it shows three doublet spectra corresponding to the three lattice sites ($k1$, $k2$, h); (b) angular variation of the spectra for a rotation of the magnetic field in the (1100) plane; (c) higher resolution of the low field spectra of panel (a) showing the resolved ^{14}N triplet HF splitting; (d) EPR photoexcitation spectrum and predicted ZPL energy range (gray) for the three axial centers (cf. Table II).

being observed in emission. This phase inversion is the result of an out-of-equilibrium spin population between the $|m_s = 0\rangle$ and $|m_s = \pm 1\rangle$ states of the $^3A_2$ ground state; it is the $|m_s = 0\rangle$ state which is preferentially populated by the photoexcitation [Fig. 2(d)]. As both EPR lines have equal intensities, the populations of the $|m_s = +1\rangle$ and $|m_s = -1\rangle$ states must be equal and much smaller than the population of the $|m_s = 0\rangle$ state. In the case of NV in diamond the optically induced ground-state spin polarization is a key property and has been attributed due to the spin-selective nonradiative recombination via two intermediate $^1A_1$ singlet states [7]. It is tempting to attribute the same process for NV centers in SiC even though calculations of the corresponding recombination paths are not yet available.

Interestingly, the related EPR spectrum is observed even at the lowest available microwave power of 200 nW in absorption instead of the first derivative form observed for the divacancies [VV^0; see Fig. 2(a)], indicating longer spin lattice relaxation time of the NV center in 3C SiC.

The relaxation time becomes even more important in the hexagonal 4H and 6H polytypes. We find that the basal, low-symmetry pairs yield less efficient ground-state spin polarization than that of the c-axis oriented (axial) NV centers with C_{3v} symmetry. We attribute this to shorter spin-lattice relaxation times and focus our further study on the axial counterparts. The spin Hamiltonian parameters for these axially symmetric NV centers, the EPR spectra of which are shown in Fig. 3 (6H) and Fig. 4 (4H), have been determined in the same way as for the 3C polytype. Again, the most important values, in particular resolved ^{14}N hyperfine splittings, are compiled in Table I: In 6H SiC we observe three $S = 1$ centers with axial C_{3v} symmetry and in 4H SiC two axial NV centers as expected from the number of nonequivalent quasicubic and hexagonal lattice sites (cf. Table I and Fig. 1). The good agreement between the calculated and the experimentally determined spin Hamiltonian parameters, namely the symmetry, electron spin S, g factor, zero-field spliting parameter D, and in particular the $A(^{14}N)$ hyperfine interactions, allow us to attribute these centers to the negatively charged $(V_{Si}N_C)^-$ defect, i.e., the

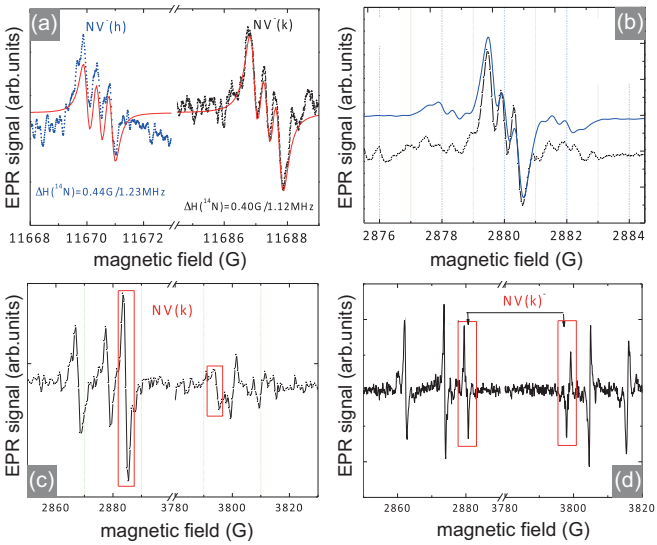

FIG. 4. 4H SiC: (a) low-field Q-band EPR spectra of the NV^- centers on h and k sites for B//c showing the ^{14}N HF splitting; experimental spectrum (dots) and fit (line) with three Lorentzian lines. (b) X-band EPR spectrum of the NV(k) center and its simulation (blue) with the calculated SHF parameters with 6 Si, 3 Si, 6 C, and 1 N neighbor atoms (see Table I). Room temperature (c) and low temperature (70 K) (d) EPR spectra, both showing the optically induced ground-state spin polarization of the NV(k) center.

TABLE II. Calculated (HSE06 functional [38]) vertical emission energies/wavelengths of the NV^- centers with axial symmetry in the three main SiC-polytypes. For comparison, values for the fundamental gap E_g (from Ref. [37]) are also given.

3*C* SiC	6*H* SiC	4*H* SiC
$E_g = 2.36$ eV	$E_g = 3.05$ eV	$E_g = 3.23$ eV
	h: 0.96 eV / 1291 nm	*h*: 0.99 eV / 1252 nm
0.86 eV / 1442 nm	*k*1: 0.95 eV / 1305 nm	*k*: 0.96 eV / 1291 nm
	*k*2: 1.00 eV / 1240 nm	

NV center in the 6*H* and 4*H* polytypes. Note that the super hyperfine (SHF) interactions calculated for three groups of three and six equivalent ^{29}Si (and six ^{13}C) nuclei are able to explain [33] the clearly visible satellite structure ≈2 G besides the central triplet lines [see Fig. 4(b)].

The calculated spin-spin contributions D^{DFT} to the ZFS are systematically slightly higher (by about 8%) than the experimentally observed values D^{exp}. With 73 ± 3 MHz in 6*H*, 111 ± 4 MHz in 4*H*, and 106 MHz in 3*C*, the deviation is larger by about a factor of 4 than for the divacancies (cf. Ref. [34]). Using the deviation of the corresponding $g_\perp$ values from the free-electron value $g_e = 2.002319$ as a measure for the intrinsic spin-orbit coupling within the respective ground state (0.0061 for NV^- and <0.0003 for VV^0), the larger discrepancies for NV^- can be rationalized by second-order spin-orbit terms which would lead to a negative correction to the ZFS. Notably, the deviation from the experimental value is almost constant for a given polytype. Hence, the differences in the ZFS parameter allow for a reliable attribution of the different spectra to specific lattice sites. In 6*H* SiC a different $S = 1$ center with much larger zero-field splitting (2.58 GHz) has been tentatively attributed to an NV center [35]. In view of the present results this assignment should be reconsidered; at least it cannot belong to the ^{3}A ground state of NV^-.

Contrary to the NV center in diamond for which the ^{3}E—^{3}A$_2$ intracenter transition is situated in the visible (632 nm), the ZPL in the three polytypes of SiC are expected to occur in the near infrared, around 1300-nm wavelength, with the exact value slightly varying with the polytype: For the two axial NV centers in 4*H* SiC, the ZPL has been experimentally determined to $\lambda = 1242$ nm by low-temperature PL spectroscopy [36]. For the 3*C* polytype with considerably smaller gap (2.36 eV instead of 3.23 for 4*H* [37]), 10% smaller ZPL energies; for the 6*H* polytype, only minor shifts of the ZPL energies as compared to the 4*H* polytype are expected [12]. Our total energy DFT calculations using the gap correcting HSE functional [38] (cf. Table II) support these suggestions.

By photo-EPR spectroscopy we have investigated the corresponding optical transitions via the spin-polarization effects. We have measured the EPR spectra at various temperatures (4–300 K) for all axial NV centers in the three polytypes as a function of laser excitation energies in the 0.95- to 2.55-eV range. Excitation with energies close to the experimental 4*H* ZPL lines leads to efficicent spin polarization with values close to 1 at low temperature ($T < 100$ K). For all five axial NV centers in 4*H* SiC and 6*H* SiC [see Fig. 3(c)] we observe optimal excitation-polarization for 980-nm excitation. Excitation with a $\lambda = 1308$ nm laser, which corresponds to an energy lower than the predicted ^{3}A$_2$—^{3}E transition, no longer spin polarizes these centers. This is in agreement with the model of polarization by recombination from the ^{3}E state. On the contrary, the ground state of the NV center in 3*C* SiC can still be spin polarized by excitation with $\lambda = 1308$ nm, once again in good agreement with the theoretical predictions (see Ref. [12] and Table II), indicating again that the ZPL energies are slightly scaling with the fundamental gap. Interestingly, the polarization effect is also observed for higher excitation energies. The responsible excitation processes are assigned to transition from the valence band to the ^{3}E state [13].

We briefly note here that the position of the Fermi level must be carefully controlled for optimal concentration of the NV center in the 1– charge state. Contrary to the case of diamond, all polytypes of SiC can be easily rendered *n*-type conductive by doping with nitrogen. For 3*C* SiC, the 1– charge state is the ground state for shallow N_C donor doped *n*-type material [12]. In the case of 4*H* and 6*H* polytypes, however, a deep (2–/–) charge transition level is predicted [12,39] and, thus, the NV centers will be in the so-called wrong, diamagnetic 2– charge state, unless the donors are at least partially compensated.

In conclusion, we have identified by EPR spectroscopy the negatively charged NV center in the polytypes 3*C*, 4*H*, and 6*H* of SiC. In agreement with theoretical predictions they display magnetic and optical properties which make them promising systems for qubit and nanosensing applications. Selective excitation of axial pairs in 4*H*/6*H* SiC will allow an easy preparation of unidirectional ensembles, thereby coping in a natural way an issue of NV centers in diamond [40,41]. The high-level technology of SiC microelectronics proposes a straightforward extension from bulk samples such as studied here to sophisticated nanopatterning and electrical-magnetic connections to control and measure the spin states. Single-spin manipulation in low-fluence irradiated layers may allow the measurement of individual spin coherence times; electron-nuclear spin coupling to the two sublattices with different nuclear magnetic moments (^{29}Si, ^{13}C) could be addressed via optically detected and time-resolved magnetic resonance spectroscopy. Finally, the incorporation of NV centers in SiC nanoparticles seems an interesting possibility for nanomagnetometry and single-photon emitter [42] applications.

The work was funded by Deutsche Forschungsgemeinschaft (DFG, SPP-1601). The computational calculations have been done at the Paderborn Center for Parallel Computing (PC^2).

[1] T. D. Ladd, F. Jelezko, R. Laflamme, Y. Nakamura, C. Monroe, and J. L. OBrien, Quantum computers, Nature (London) **464**, 45 (2010).

[2] D. D. Awschalom, L. C. Bassett, A. S. Dzurak, E. L. Hu, and J. R. Petta, Quantum spintronics : Engineering and manipulating atom-like spins in semiconductors, Science **339**, 1174 (2013).

[3] L. du Preez, Ph.D. thesis, University of Witwatersrand, Johannesburg, 1965 (unpublished).

[4] F. Jelezko and J. Wrachtrup, Single defect centers in diamond: A review, Phys. Stat. Sol. A **203**, 3207 (2006).

[5] A. Gruber, A. Dräbenstedt, C. Tietz, L. Fleury, J. Wrachtrup and C. von Borczyskowski, Scanning confocal optical microscopy and magnetic resonance on single defect centers, Science **276**, 2012 (1997).

[6] M. W. Doherty, N. B. Manson, P. Delaney, F. Jelezko, J. Wrachtrup, and L. C. L. Hollenberg, The nitrogen vacancy colour center in diamond, Phys. Rep. **528**, 1 (2013).

[7] M. L. Goldman, M. W. Doherty, A. Sipahigil, N. Y. Yao, S. D. Bennett, N. B. Manson, A. Kubanek, and M. D. Lukin, State selective intersystem crossing in nitrogen vacancy centers, Phys. Rev. B **91**, 165201 (2015).

[8] J. R. Weber, W. F. Koehl, J. B. Varley, A. Janotti, B. B. Buckley, C. G. van de Walle, and D. D. Awschalom, Quantum computing with defects, Proc. Natl. Acad. Sci. USA **107**, 8513 (2010).

[9] D. DiVincenzo, Better than excellent, Nat. Mater. **9**, 468 (2010).

[10] A. Dzurak, Quantum computing: Diamond and silicon converge, Nature (London) **479**, 47 (2011).

[11] A. Boretti, Optical materials: silicon carbide's quantum aspects, Nat. Photonics **8**, 88 (2014).

[12] L. Gordon, A. Janotti, and C. G. Van de Walle, Defects as qubits in 3C- and 4H-SiC, Phys. Rev. B **92**, 045208 (2015).

[13] A. Gali, A. Gällström, N. Son, and E. Janzén, Theory of neutral divacancy in SiC: A defect for spintronics, Mater. Sci. Forum **645**, 395 (2010).

[14] A. Gali, Time-dependent density functional study on the excitation spectrum of point defects in semiconductors, Phys. Status Solidi (B) **248**, 1337 (2011).

[15] W. F. Koehl, B. B. Buckley, F. J. Heremans, G. Calusine, and D. D. Awschalom, Room temperature coherent control of defect spin qubits in silicon carbide, Nature (London) **479**, 84 (2011).

[16] V. A. Soltamov, A. A. Soltamova, P. G. Baranov, and I. I. Proskuryakov, Room Temperature Coherent Spin Alignment of Silicon Vacancies in 4H- and 6H-SiC, Phys. Rev. Lett. **108**, 226402 (2012).

[17] H. Kraus, V. A. Soltamov, D. Riedel, S. Väth, F. Fuchs, A. Sperlich, P. G. Baranov, V. Dyakonov, and G. V. Astakhov, Room-temperature quantum microwave emitters based on spin defects in silicon carbide, Nat. Phys. **10**, 157 (2014).

[18] D. J. Christle, A. L. Falk, P. Andrich, P. V. Klimov, J. U. Hassan, N. T. Son, E. Janzén, T. Ohshima, and D. D. Awschalom, Isolated electron spins in silicon carbide with millisecond coherence times, Nat. Mater. **14**, 160 (2015).

[19] M. Widmann, S.-Y. Lee, T. Rendler, N. T. Son, H. Fedder, S. Paik, L. Yang, N. Zhao, S. Yang, I. Booker, A. Denisenko, M. Jamali, S. A. Momenzadeh, I. Gerhardt, T. Ohshima, A. Gali, E. Janzén, and J. Wrachtrup, Coherent control of single spins in silicon carbide at room temperature, Nat. Mater. **14**, 164 (2015).

[20] S. Castelletto, B. C. Johnson, V. Ivády, N. Stavrias, T. Umeda, A. Gali, and T. Ohshima, A silicon carbide room-temperature single-photon source, Nat. Mater. **13**, 151 (2014).

[21] H. J. von Bardeleben, J. L. Cantin, E. Rauls, and U. Gerstmann, Identification and magneto-optical properties of the NV center in 4H-SiC, Phys. Rev. B **92**, 064104 (2015).

[22] A. Oliveros, A. Giuseppi-Elie, and S. E. Saddow, Silicon carbide: A versatile material for biosensor applications, Biomed. Microdevices **15**, 353 (2013).

[23] B. Somogyi, V. Zólyomi, and A. Gali, Near-infrared luminescent cubic silicon carbide nanocrystals for in vivo biomarker applications: An ab initio study, Nanoscale **4**, 7720 (2012).

[24] J. P. Perdew, K. Burke, and M. Ernzerhof, Generalized Gradient Approximation Made Simple, Phys. Rev. Lett. **78**, 1396 (1997).

[25] P. E. Blöchl, Projector augmented-wave method, Phys. Rev. B **50**, 17953 (1994).

[26] P. Giannozzi *et al.*, QUANTUM ESPRESSO: A modular and open source software project for quantum simulations of materials, J. Phys.: Condens. Matter **21**, 395502 (2009)[www.quantum-espresso.org].

[27] C. J. Pickard and F. Mauri, First Principle Theory of the EPR *g*-Tensor in Solids: Defects in Quartz, Phys. Rev. Lett. **88**, 086403 (2002).

[28] V. Ivády, T. Simon, J. R. Maze, I. A. Abrikosov, and A. Gali, Pressure and temperature dependence of the zero-field splitting in the ground state of NV centers in diamond: A first-principles study, Phys. Rev. B **90**, 235205 (2014).

[29] Z. Bodrog and A. Gali, The spin-spin zero-field splitting tensor in the projector-augmented-wave method, J. Phys.: Condens. Matter **26**, 015305 (2014).

[30] G. Kresse and J. Furthmüller, Efficient iterative schemes for *ab initio* total energy calculations using a plane wave basis set, Phys. Rev. B **54**, 11169 (1996).

[31] U. Gerstmann, E. Rauls, Th. Frauenheim, and H. Overhof, Formation and annealing of nitrogen complexes in 3C-SiC, Phys. Rev. B **67**, 205202 (2003).

[32] A. L. Falk, B. B. Buckley, G. Calusine, W. V. V. Dobrovitski, A. Politi, C. A. Zorman, P. X. L. Feng, and D. D. Awschalom, Polytype control of spin qubits in silicon carbide, Nat. Commun. **4**, 1819 (2013).

[33] Experimentally, slightly (by ≈1 MHz) larger ^{29}Si SHF are suggested by the spectra taken at 70 K; the DFT values in Table I are calculated for 0 K. We thus attribute this SHF discrepancy to a thermal charge redistribution from the carbon dangling bonds to the outer Si ligands.

[34] A. L. Falk, P. V. Klimov, V. Ivády, K. Szász, D. J. Christle, W. F. Koehl, A. Gali, and D. D. Awschalom, Optical Polarization of Nuclear Spins in Silicon Carbide, Phys. Rev. Lett. **114**, 247603 (2015).

[35] M. V. Muzafarova1a, I. V. Ilyin, E. N. Mokhov, V. I. Sankin, and P. G. Baranov, Identification of the triplet state N-V defect in neutron irradiated silicon carbide by electron paramagnetic resonance, Mat. Sci. Forum **527**, 555 (2006).

[36] S. A. Zargaleh, B. Eble, S. Hameau, J.-L. Cantin, L. Legrand, M. Bernard, F. Margaillan, J.-S. Lauret, J.-F. Roch, H. J. von Bardeleben, E. Rauls, U. Gerstmann, and F. Treussart, Evidence for near infrared photoluminescence of the nitrogen vacancy center in 4H SiC, Phys. Rev. B **94**, 060102(R) (2016).

[37] Y.-S. Park, in *SiC Materials and Devices* (Academic Press, San Diego, 1998), p. 2060.

[38] J. Heyd and G. E. Scuseria, Efficient hybrid density functional calculations in solids: Assessment of the Heyd-Scuseria-Ernzerhof screened Coulomb hybrid functional, J. Chem. Phys. **121**, 1187 (2004).

[39] J. R. Weber, W. F. Koehl, J. B. Varley, A. Janotti, B. B. Buckley, C. G. Van de Walle, and D. D. Awschalom, Defects in SiC for quantum computing, J. Appl. Phys. **109**, 102417 (2011).

[40] A. M. Edmonds, U. F. S. D'Haenens-Johansson, R. J. Cruddace, M. E. Newton, K.-M. C. Fu, C. Santori, R. G. Beausoleil, D. J. Twitchen, and M. L. Markham, Production of oriented nitrogen-vacancy color centers in synthetic diamond, Phys. Rev. B **86**, 035201 (2012).

[41] T. Miyazaki, Y. Miyamoto, T. Makino, H. Kato, S. Yamasaki, T. Fukui, Y. Doi, N. Tokuda, M. Hatano, and N. Mizuochi, Atomistic mechanism of perfect alignment of nitrogen-vacancy centers in diamond, Appl. Phys. Lett. **105**, 261601 (2014).

[42] S. Castelletto, B. C. Johnson, C. Zachreson, D. Beke, I. Balogh, T. Ohshima, I. Aharonovich, and A. Gali, Room temperature quantum emission from cubic silicon carbide nanoparticles, ACS Nano **8**, 7938 (2014).